PAPER

Molecular phase engineering of organic semiconductors based on a [1]benzothieno[3,2-b][1]benzothiophene core†

Yaowu He,[a] Wenjun Xu,[a] Imran Murtaza,[bc] Dongwei Zhang,[a] Chao He,[a] Yanan Zhu[a] and Hong Meng[*ab]

Two environmentally and thermally stable [1]benzothieno[3,2-b][1]benzothiophene (BTBT) derivatives, 2-phenyl[1]benzothieno[3,2-b][1]benzothiophene (Ph-BTBT) and 2-(4-hexylphenyl)[1]benzothieno[3,2-b][1]benzothiophene (C6-Ph-BTBT), are prepared by Suzuki coupling. Organic thin-film transistors with a top-contact and bottom-gate based on BTBT, Ph-BTBT and C6-Ph-BTBT are fabricated by vacuum-deposition on octyltrichlorosilane treated Si/SiO_2 substrates. Experimental results show that the thin-film based on BTBT sublimes instantly after the deposition of electrodes, and no semiconductor signal is detected. Ph-BTBT shows a mobility of 0.034 cm^2 V^{-1} s^{-1}. Furthermore, C6-Ph-BTBT exhibits three liquid crystal phases (Sm A, Sm E and Sm K or H) and achieves the highest hole mobility of 4.6 cm^2 V^{-1} s^{-1} with an on/off ratio of 2.2 × 10^7 for polycrystalline organic thin-film transistors in ambient air. The present study exemplifies that the introduction of mesoscopic order in molecular design provides a general approach for the high electronic performance of organic semiconductors.

Introduction

Organic thin-film transistors (OTFTs) have attracted significant attention due to their great potential in electronic applications, including chemical sensors, electronic paper and active-matrix displays.[1] To date, many high performance OTFTs have been developed based on the advancement in fabrication techniques and the development of organic semiconductors.[2] Many reported organic semiconductors exhibit higher mobility than amorphous silicon. In particular, thienoacenes are commonly used in organic semiconductors, which often present excellent environmental stability with high mobility, such as [1]benzothieno[3,2-b][1]benzothiophene (BTBT) derivatives. Diphenyl-substituted BTBT and dialkyl-substituted BTBT have been reported to have higher hole mobilities than 1 cm^2 V^{-1} s^{-1}.[3] C13-BTBT and C8-BTBT have been recently reported with the high mobility values of 17.2 and 43 cm^2 V^{-1} s^{-1}, respectively.[4] However, the development of high performance organic semiconductors with excellent environmental and thermal stabilities is still a challenge for the practical applications of OTFTs.

In recent years, liquid-crystalline materials have been considered as promising candidates for OTFTs due to the formation of well-ordered polycrystalline thin-films with large aligned domains, depending on the deposition technique or the thermal annealing temperature in the liquid crystal phase.[5] Besides, highly ordered mesophases (such as smectic E and smectic G phases) are often considered in OTFT materials. The expected liquid crystals for OTFTs need to exhibit higher ordered liquid crystalline phases, such as smectic E (Sm E) or smectic G (Sm G) phases, close to the crystal phase. These higher ordered phases can effectively satisfy the formation of well-ordered uniform thin films due to their solid-like nature.[6] The mobilities of a series of liquid crystalline compounds are summarized in Table S1.† For example, Meng *et al.* reported liquid crystals of DHTAnt, and they showed the mobility of 0.5 cm^2 V^{-1} s^{-1}, which is about 10 times larger than non-liquid crystals of DTAnt.[7] In 2012, Iino *et al.* reported the BTBT core based liquid crystalline material 8-TP-BTBT, which exhibited a mobility as high as 1.4 ± 0.3 cm^2 V^{-1} s^{-1} in the Sm E phase.[8] Afterwards, they found a similar compound, Ph-BTBT-10, with self-assembling ability, which is able to form a uniform and molecularly smooth polycrystalline thin film using the Sm E precursor. Ph-BTBT-10 based OTFTs have achieved mobilities as high as 14.7 cm^2 V^{-1} s^{-1}.[5g]

It is known that long alkyl chain substituted BTBT derivatives often show higher mobility. Similar results have been reported for oligothiophene and DNTT derivatives.[9] Despite the fact that there are studies on the high charge mobility of BTBT derivatives, the charge transfer property of the BTBT core itself

[a]School of Advanced Materials, Peking University Shenzhen Graduate School, Shenzhen, 518055, China. E-mail: menghong@pkusz.edu.cn
[b]Key Laboratory of Flexible Electronics (KLOFE), Institute of Advanced Materials (IAM), Jiangsu National Synergetic Innovation Center for Advanced Materials (SICAM), Nanjing Tech University (Nanjing Tech), 30 South Puzhu Road, Nanjing 211816, China
[c]Department of Physics, International Islamic University, Islamabad 44000, Pakistan
† Electronic supplementary information (ESI) available. See DOI: 10.1039/c6ra22999a

has not yet reported in the literature. Our experiments show that its thin-films sublime instantly after the deposition of electrodes, thus explaining why BTBT is not used as the active layer in OTFTs. In order to explore new semiconductors based on the BTBT core and understand the alkyl chain effects, we designed and synthesized 2-phenyl[1]benzothieno[3,2-*b*][1]benzothiophene (Ph-BTBT) and 2-(4-hexylphenyl)[1]benzothieno[3,2-*b*][1]benzothiophene (C6-Ph-BTBT). The phenyl unit enhances the molecular density and thermal stability, whereas the alkyl chain allows control of the mesoscopic organization of the molecule.

In the present study, we comparatively study the optical and electronic properties of two semiconductors and demonstrate that the higher ordered liquid crystalline phases play an important role in determining the high charge mobility of the semiconductors. The two materials show similar electrochemical and optical properties, but present significant differences in OTFT performance. Ph-BTBT exhibits a hole mobility of only 0.034 cm^2 V^{-1} s^{-1}. In contrast, the alkyl chain substituted C6-Ph-BTBT shows a considerable performance with great dependence on the substrate and annealing temperature. The mobility is enhanced from 0.34 ± 0.05 to 2.3 ± 0.2 cm^2 V^{-1} s^{-1} with an increase in the substrate temperature from 25 to 80 °C. In particular, the OTFTs deposited at 100 °C reaches the highest mobility of 4.6 cm^2 V^{-1} s^{-1} after annealing at 80 °C.

Results and discussion

Synthesis

Scheme 1 shows the synthetic route of Ph-BTBT and C6-Ph-BTBT. The intermediate compounds 2-bromo[1]benzothieno[3,2-*b*]benzothiophene (5) and 2-(4-hexylphenyl)-4,4,5,5-tetramethyl-1,3,2-dioxaborolane (6b) were prepared using previous literature procedures.[10] 2-Bromo[1]benzothieno[3,2-*b*]benzothiophene (5) and intermediate compounds 6a or 6b were processed by a palladium-catalyzed Suzuki–Miyaura coupling reaction to obtain the target compounds Ph-BTBT and C6-Ph-BTBT in high

yield. The sublimation process was employed to obtain the pure white solid of titled compounds. Finally, their chemical structures were confirmed by NMR and HRMS.

Electronic properties

Cyclic voltammetry (CV) and UV-vis spectroscopy were applied to investigate the HOMO and LUMO energy and optical band gaps (E_g). The optical band gap (E_g) was measured by UV-vis spectroscopy. Fig. 1a shows the UV-vis absorption spectra of Ph-BTBT and C6-Ph-BTB. As can be seen, the maximum absorption edges for both Ph-BTBT and C6-Ph-BTBT in dichloromethane solution are at 361 nm. Therefore, the energy gaps of C6-Ph-BTBT and Ph-BTBT are calculated to be 3.43 eV each. The absorption edge wavelengths (λ_{edge}) of the two materials in solution are longer than that in the thin-films. This result indicates that there is J-aggregation in the thin-films which is analogous with previous studies.[11] In addition, both C6-Ph-BTBT and Ph-BTBT show blue emission, since all the peaks of their fluorescence spectra are located between 480 nm to 650 nm (Fig. S1b†). CV was applied to obtain the electronic states of C6-Ph-BTBT and further to analyze the stability and charge injection process. The redox properties of C6-Ph-BTBT and Ph-BTBT are shown in Fig. 1b. The onsets of oxidation peaks of C6-Ph-BTBT, Ph-BTBT and ferrocene were employed to obtain the highest occupied molecular orbital (HOMO) levels of −5.65 and −5.68 eV for C6-Ph-BTBT and Ph-BTBT, respectively.[12] The lowest unoccupied molecular orbital (LUMO) level of C6-Ph-BTBT and Ph-BTBT were calculated to be −2.22 and −2.25 eV, respectively, based on the HOMO level and their bandgaps. The experimental results show that the energy levels of Ph-BTBT and C6-Ph-BTBT are not obviously different and the high HOMO levels indicate that the two organic semiconductor materials are very stable in air. Moreover, both Ph-BTBT and C6-Ph-BTBT exhibit high thermal stability, as demonstrated by thermogravimetry analysis (TGA), which shows that their decomposition temperatures at 308 and 327 °C (Fig. S1a†), respectively.
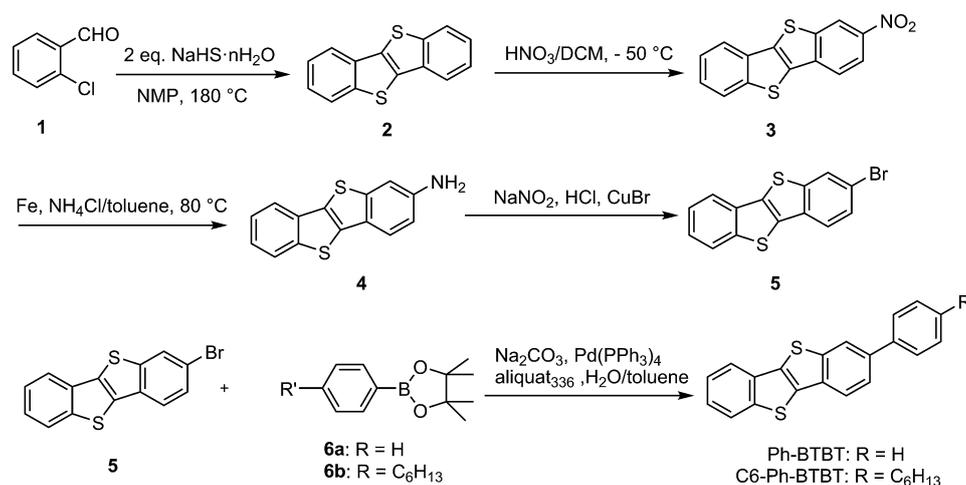
Scheme 1 Synthetic approach for the BTBT derivatives.
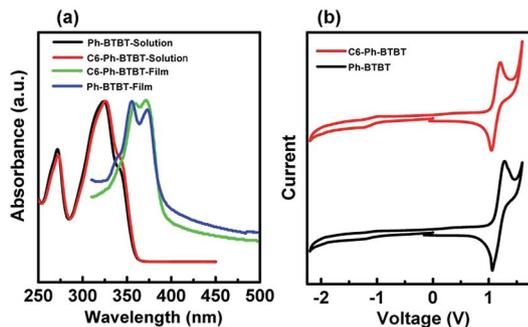
Fig. 1 (a) UV-vis spectra of Ph–BTBT and C6-Ph–BTBT; and (b) cyclic voltammogram of Ph–BTBT and C6-Ph–BTBT in dichloromethane.

Fig. 3 DSC curves of Ph–BTBT and C6-Ph–BTBT.

Thermal properties

The thermal properties of Ph-BTBT and C6-Ph-BTBT were investigated by differential scanning calorimetry (DSC). The DSC curves of Ph-BTBT and C6-Ph-BTBT are shown in Fig. 3. As can be seen, only one transition can be observed in the DSC trace of Ph-BTBT for heating processes. However, for C6-Ph-BTBT, there are four transitions in its DSC trace for both cooling and heating processes. Judging from this phenomenon, C6-Ph-BTBT shows liquid crystal behavior at high temperature conditions. In the cooling curve of C6-Ph-BTBT, the first exothermic peak is located at 222.5 °C. This represents the transition from isotropic-to-Sm A (enthalpy, $\Delta H = 10.45$ J g^{-1}), which is confirmed by the polarized optical microscopy (POM) observation on the basis of the typical fan-shaped texture of the Sm A phase (Fig. 2a).[13] In addition, a high enthalpy ($\Delta H = 17.93$ J g^{-1}) is observed at the second peak which is located at 185.6 °C. This indicates a transition from Sm A to an ordered phase (Sm E), which is also confirmed by the POM observation depending on the typical striated fan-shaped texture of the Sm E phase (Fig. 2b). Additionally, a larger enthalpy ($\Delta H = 29.37$ J g^{-1}) is observed at the third exothermic peak which is located at 152.9 °C. This represents a transition from Sm E to a higher ordered phase. Moreover, a small enthalpy ($\Delta H = 1.44$ J g^{-1}) is detected in the fourth exothermic peak at 54.4 °C. This indicates the transition from a soft crystal to a crystal. It should be the Sm K or H phase according to the decrease in entropy of the liquid crystal phase.[14] In the previous literature, large domains can be observed when the Sm E phase was cooled to soft crystal (e.g. Sm
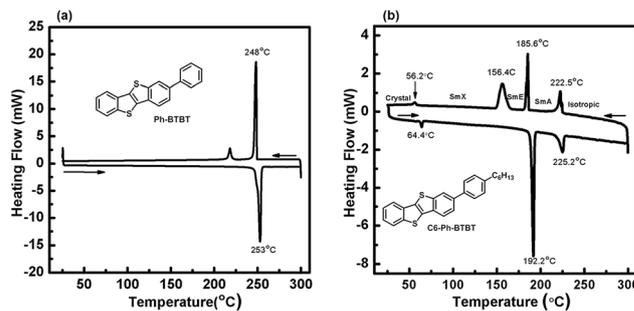
G) and maintained at room temperature. In our case, the transition is consistent with the literature, as depicted by the POM textures of C6-Ph-BTBT in Fig. 2c (Sm K or H phase) and Fig. 2d (crystal phase). As can be seen, the phases of Sm K or H and crystal do not present an obvious difference in these two figures. This phenomenon indicates that the highly ordered molecular packing of the Sm K or H phase is able to be retained at room temperature.

Charge transport properties

To investigate and compare the field-effect properties of the Ph-BTBT and C6-Ph-BTBT materials, top-contact/bottom-gate OTFTs were fabricated by vacuum-deposition (50 nm) on octyltrichlorosilane (OTS (8)) treated Si/SiO$_2$ (250 nm SiO$_2$) substrates. The liquid-crystalline materials can form well-ordered polycrystalline thin films as-deposited or after thermal annealing at the temperature of the liquid crystal phase, which can improve the mobility of OTFT devices. To achieve a better device performance various substrate temperatures (T_{sub}) and annealing temperatures (T_{anneal}) were selected.

The performance characteristics of the devices were measured under ambient conditions. In addition, the standard metal-oxide-semiconductor field-effect transistor (MOSFET) equations were chosen to calculate the mobility (μ), and on/off current ratio (I_{on}/I_{off}) in the saturation regime. The results of the Ph-BTBT and C6-Ph-BTBT based OTFT performances are summarized in Tables 1 and 2. Fig. 4 and S4–S6† show the typical output and transfer characteristics of the OTFTs based on Ph-BTBT and C6-Ph-BTBT. All of the devices show typical p-channel OTFT responses. As can be seen, the OTFTs transfer
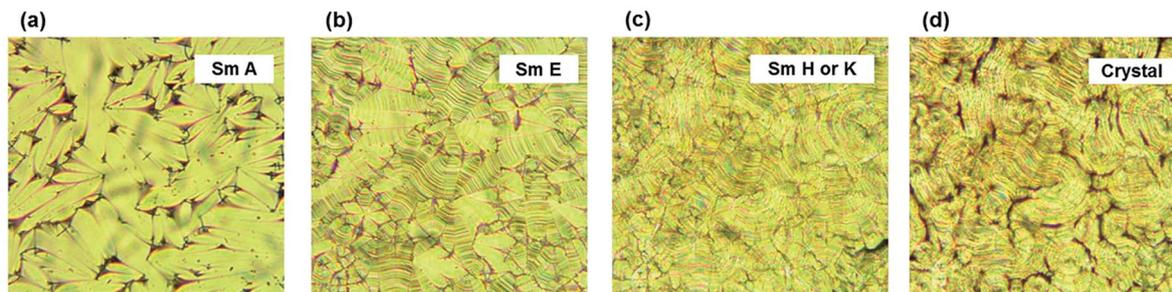
Fig. 2 Polarized optical microscopy images of C6–Ph–BTBT. (a) Sm A phase, (b) Sm E phase, (c) Sm K or H phase and (d) crystal phase.

Table 1 OTFTs performances of Ph-BTBT and C6-Ph-BTBT

Comp.	Temp.[a]	μ_{sat} [cm^2 V^{-1} s^{-1}]	I_{on}/I_{off}
Ph-BTBT[b]	25 °C	0.012 ± 0.004 (0.016)	(1.2 ± 2.6) × 10^5
	60 °C	0.016 ± 0.016 (0.034)	(5.8 ± 4.1) × 10^4
C6-Ph-BTBT[c]	25 °C	0.34 ± 0.05 (0.41)	(2.7 ± 1.3) × 10^6
	60 °C	1.6 ± 0.3 (2.2)	(3.1 ± 2.6) × 10^6
	80 °C	2.3 ± 0.2 (2.7)	(7.8 ± 3.4) × 10^6
	100 °C	2.1 ± 0.1 (2.4)	(7.4 ± 4.2) × 10^6
	120 °C	0.94 ± 0.42 (1.6)	(2.4 ± 1.9) × 10^6

[a] Substrate temperature. [b] All data are reported as the average value of more than 3 devices. [c] All data are reported as the average value of 10 devices. The values in parenthesis represent the maximum mobility.

characteristics are strongly dependent on the substrate and annealing temperatures. At T_{sub} = 25 °C, the OTFTs based on Ph-BTBT show the mobility of 0.012 ± 0.004 cm^2 V^{-1} s^{-1} and on/off ratios of 1.2 × 10^5. The mobility is very low and the standard deviation of μ_{TFT} between these OTFTs was relatively large due to the effect of non-uniform thin-films (see the following discussion on film morphology). Furthermore, the OTFTs device performances have no significant improvement

with an increase in substrate temperature (T_{sub} = 60 °C, μ = 0.016 ± 0.016 cm^2 V^{-1} s^{-1}). As we predicted, the OTFTs based on C6-Ph-BTBT show higher mobility than that of Ph-BTBT. Thus, the introduction of an alky chain (C$_6$H$_{13}$) on the BTBT core can improve the OTFTs characteristics. Furthermore, C6-Ph-BTBT tends to have better OTFTs device performances in the devices fabricated at higher substrate temperatures, and the maximum mobility was detected at T_{sub} = 80 °C. According to the DSC curve, the phase of C6-Ph-BTBT at this temperature should belong to the liquid crystal phase. This phenomenon indicates that the OTFTs can obtain higher mobility if the thin films are fabricated at the temperature of the liquid crystal phase. The maximum mobility of 2.7 cm^2 V^{-1} s^{-1} with an average of 2.3 ± 0.2 cm^2 V^{-1} s^{-1} is obtained, which is higher than that of the mobility of DPh-BTBT (2.0 cm^2 V^{-1} s^{-1}).[3a]

On the other hand, the OTFTs annealed at higher temperatures exhibit a better performance. The OTFTs as deposited (T_{sub} = 25 °C) without annealing can reach the maximum mobility of 0.41 cm^2 V^{-1} s^{-1} with an average of 0.34 ± 0.0005 cm^2 V^{-1} s^{-1}. Note that the mobility of the OTFTs fabricated under this condition varies with a relatively large standard deviation due to the non-uniformity of the thin films. The

Table 2 OTFT performance of the C6-Ph-BTBT-based devices after annealing at various temperatures

T_{anneal}[b]	T_{sub}[a] = 25 °C			T_{sub} = 100 °C		
	μ_{sat}[c] [cm^2 V^{-1} s^{-1}]	I_{on}/I_{off}	V_{th} [V]	μ_{sat}[b] [cm^2 V^{-1} s^{-1}]	I_{on}/I_{off}	V_{th} [V]
25 °C	0.34 ± 0.05 (0.41)	(2.7 ± 1.3) × 10^6	−26.4 ± 1.4	2.1 ± 0.1 (2.4)	(7.4 ± 4.2) × 10^6	−36.1 ± 0.7
80 °C	0.81 ± 0.17 (1.2)	(6.8 ± 0.8) × 10^6	−16.1 ± 2.2	4.0 ± 0.4 (4.6)	(1.9 ± 0.8) × 10^7	−27.4 ± 2.7
100 °C	1.3 ± 0.2 (1.7)	(9.8 ± 2.9) × 10^6	−27.0 ± 3.3	1.9 ± 0.3 (2.4)	(1.2 ± 0.6) × 10^7	−34.0 ± 3.0
120 °C	0.69 ± 0.08 (0.79)	(6.1 ± 2.6) × 10^6	−32.7 ± 1.8	0.93 ± 0.25 (1.4)	(5.6 ± 1.8) × 10^6	−37.5 ± 2.1

[a] Substrate temperature. [b] The devices were thermally annealed at various temperatures. [c] All data are reported as the average value of 10 devices. The values in parenthesis represent the maximum mobility.
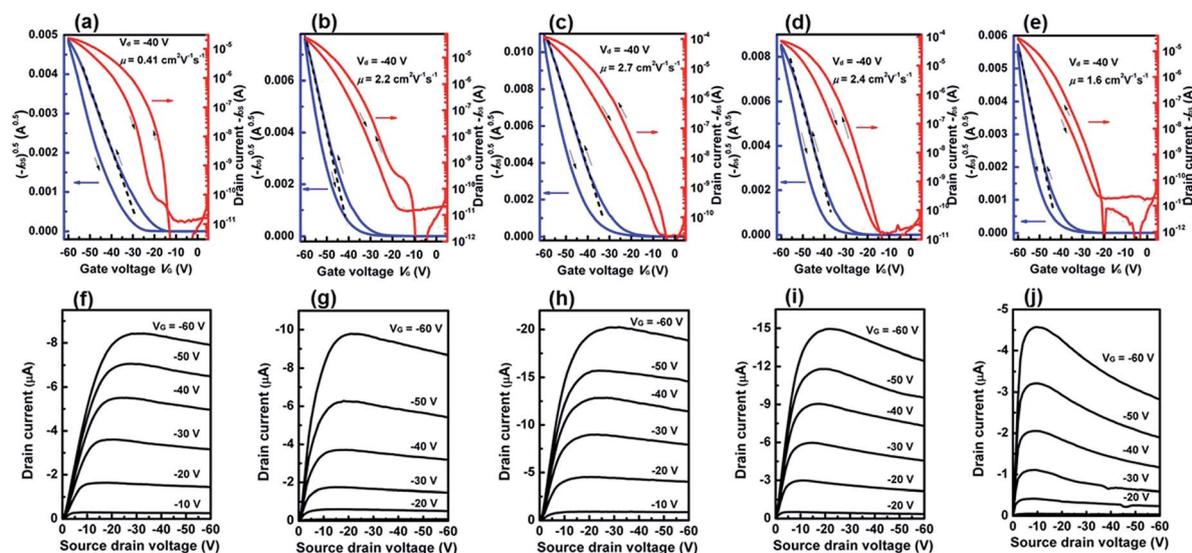
Fig. 4 Transfer and output curves of OTFTs of C6-Ph-BTBT films grown on an OTS-coated substrate at T_{sub} = 25 °C (a, f), 60 °C (b, g), 80 °C (c, h), 100 °C (d, i), and 120 °C (e, j). (a), (b), (c), (d) and (e) I_{DS}−V_G characteristics curves; (f), (g), (h), (i) and (j) I_{DS}−V_{DS} characteristics curves.

OTFTs annealed at 80 °C (liquid crystal phase) exhibit a higher mobility of up to 0.81 ± 0.17 cm^2 V^{-1} s^{-1} with an on–off ratio of 6.8×10^6. Surprisingly, the OTFTs performance improves up to 1.3 ± 0.2 cm^2 V^{-1} s^{-1} after thermal annealing at 100 °C (liquid crystal phase). The maximum mobility obtained is 1.7 cm^2 V^{-1} s^{-1} with an I_{on}/I_{off} of 9.5×10^6. However, the OTFTs mobility decreases to 0.69 ± 0.08 cm^2 V^{-1} s^{-1} after thermal annealing at 120 °C. As can be seen from Fig. S6e–g,† the contact resistance of the OTFTs based on C6-Ph-BTBT gradually decreases as the annealing temperature increases up to $T_{sub} = 100$ °C.

As can be seen from Fig. S5e–g,† the contact resistance of the OTFTs based on C6-Ph-BTBT gradually decreases as the annealing temperature increase up to $T_{sub} = 100$ °C. The mobility of the OTFTs based on C6-Ph-BTBT is obviously enhanced by thermal annealing. The maximum mobility of 4.6 cm^2 V^{-1} s^{-1} with an average of 4.0 ± 0.4 cm^2 V^{-1} s^{-1} is obtained after thermal annealing at 80 °C. It is worth noting that threshold voltages of all the devices are relatively large due to the existence of contact resistance and mismatch of the HOMO level of organic semiconductors with the work function of gold (5.2 eV), which forms a barrier for charge injection.

Morphological characterizations

The relationships of molecular structures with the thin film morphology, and the OTFTs performance with the substrate temperatures the morphology of thin films of Ph-BTBT and C6-Ph-BTBT deposited at different substrate temperatures was investigated by atomic force microscopy (AFM) and thin film X-ray diffraction (XRD). As shown in Fig. 5a, in contrast to the thin film of Ph-BTBT deposited at $T_{sub} = 25$ °C, which shows a heterogeneous morphology with a surface roughness of 14.9 nm (R_q), the C6-Ph-BTBT thin films, grown at the same condition, show a homogenous morphology with a lower surface roughness of 2.67 nm (Fig. 5b). Consistent with the film morphologies, the OTFTs based on Ph-BTBT show low mobility while those based on C6-Ph-BTBT exhibit higher mobility.
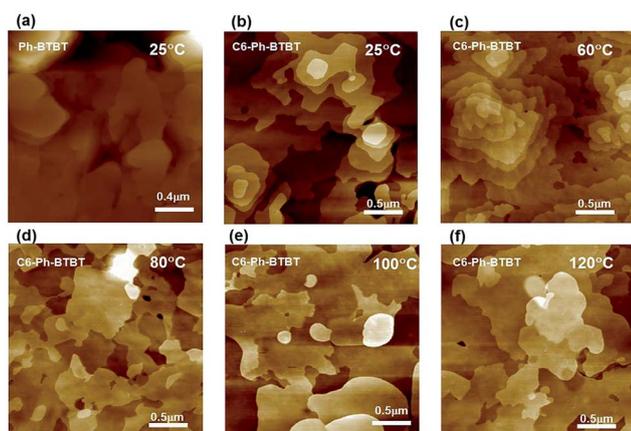
The substrate temperature influences the morphology of the thin films of C6-Ph-BTBT. Fig. 4c–f show AFM images of the thin films of C6-Ph-BTBT deposited at $T_{sub} = 60$, 80, 100 and 120 °C, respectively. The domain size of the thin films based on C6-Ph-BTBT is largely influenced by substrate temperature, where the size becomes progressively larger with an increase in substrate temperature. Ordinarily, larger grains are conducive to improve the carrier mobility.[15] This result is consistent with the stronger field-effect response in the actual devices. A highly regular terrace structure is observed at room temperature and each step height of the terrace is measured to be approximately 2.36 nm, which corresponds to the molecules along the long molecular axis of C6-Ph-BTBT (2.5 nm calculated by B3LYP/6-31+G(d,p)[16]). This indicates a near-perpendicular alignment of the molecules with respect to the substrate surface. Fig. 5c shows an AFM image of the surface of the thin film deposited at $T_{sub} = 60$ °C. The surface of the thin film becomes smoother than before due to molecular movements such as the rotation around the molecular axis and the translational diffusion in high temperature condition. This phenomenon should promote the formation of high-quality thin films. Interestingly, the terrace structures disappear and the surface of the film surprisingly becomes uniform at $T_{sub} = 80$ °C, as shown in Fig. 5d. This indicates that the domains are highly ordered and have low defect density. We can predict that the characteristics of the OTFTs fabricated at this condition will reach a higher performance due to the uniformity of the thin-films. With a further increase in the substrate temperature to $T_{sub} = 120$ °C, a large number of cracks occur on the thin-films, as shown in Fig. 5f. These cracks are detrimental to carrier mobility, which is consistent with the weaker field-effect response in the actual devices. All these phenomena are consistent with the OTFTs based on C6-Ph-BTBT device performance, which allow us to conclude that with an increase in the substrate temperature a great improvement in thin-film morphology is presented for the C6-Ph-BTBT material. From the experiments, the OTFTs performance shows a direct correlation with the uniformity of the thin-films. For example, the films deposited at 80 °C have the lowest roughness with the corresponding highest mobility of 2.7 cm^2 V^{-1} s^{-1}.

Fig. 6 shows the XRD pattern of the thin film based on C6-Ph-BTBT deposited at different substrate temperatures. The XRD patterns of C6-Ph-BTBT show higher order reflections with the

Fig. 5 AFM height images of thin-films. (a) Ph–BTBT as-grown film, and the films of C6-Ph-BTBT deposited at different substrate temperatures: (b) as-grown, (c) 60 °C, (d) 80 °C, (e) 100 °C, and (f) 120 °C.
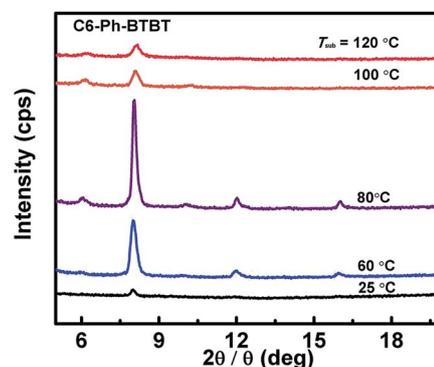
Fig. 6 XRD pattern of thin film based on C6-Ph-BTBT as deposited at various substrate temperatures.

increase in substrate temperature, which indicate better ordering in the films grown at higher substrate temperatures. At $T_{sub} = 80\ ^\circ$C, the XRD pattern of C6-Ph-BTBT shows the highest order reflection. These results are consistent with the AFM morphology and OTFTs performance.

Conclusions

In summary, we have successfully synthesized a non-liquid crystalline material, Ph-BTBT, and a liquid crystalline material, C6-Ph-BTBT, and fabricated OTFTs based on them. Ph-BTBT shows the low mobility of 0.034 cm^2 V^{-1} s^{-1}, however C6-Ph-BTBT exhibits over two orders of magnitude higher mobility than that of Ph-BTBT under the same conditions. For C6-Ph-BTBT, we have found that the substrate and annealing temperature presents a great effect on the OTFTs performance. At $T_{sub} = 25\ ^\circ$C, the OTFTs show the mobility of 0.41 cm^2 V^{-1} s^{-1}. It is intriguing that the mobility of the OTFTs is dramatically enhanced up to 2.7 cm^2 V^{-1} s^{-1} if the substrate temperature is increased to 80 $^\circ$C. Surprisingly, the OTFTs based on C6-Ph-BTBT fabricated at $T_{sub} = 100\ ^\circ$C reached the maximum mobility of 4.6 cm^2 V^{-1} s^{-1} after annealing at 80 $^\circ$C. Besides the Sm E phase, the higher ordered liquid crystalline phase of Sm K or H was observed for the first time in BTBT based semiconductors. We conclude that the liquid crystal material of C6-Ph-BTBT can be fabricated in the form of satisfactory polycrystalline thin films with high uniformity for OTFTs, as compared with the non-liquid crystal material of Ph-BTBT. This directly shows the great potential of C6-Ph-BTBT for future applications in organic electronics. Further chemical engineering to achieve more soluble materials is in progress in our lab.

Experimental

General

All chemicals and solvents are analytical reagents unless otherwise noted. All reactions were performed under a nitrogen atmosphere in dry solvent. The synthetic route of Ph-BTBT and C6-Ph-BTBT is shown Scheme 1. Thermo-gravimetric analysis (TGA) was carried out on a TA Instruments TA2950 TGA system at a heating rate of 10 $^\circ$C min^{-1} and a nitrogen flow rate of 60 cm^3 min^{-1}. Differential scanning calorimetry (DSC) was run on a TA Instruments DSC Q1000 at a heating or cooling rate of 5 $^\circ$C min^{-1} under a nitrogen flow. The liquid crystal behavior of C6-Ph-BTBT was characterized with a POM equipped with a Mettler-Toledo FP82 HT hot-stage. XRD patterns were recorded using a Bruker D8 advance X-ray diffractometer with a Cu K$_\alpha$ source ($\lambda = 1.541$ Å). Film morphology was studied via atomic force microscopy (AFM) on an SPA400HV instrument with an SPI 3800 controller (Seiko Instruments).

2-(4-Hexylphenyl)-4,4,5,5-tetramethyl-1,3,2-dioxaborolane (7b)

^{1}H NMR (300 MHz, CDCl$_3$) δ 7.74 (d, $J = 7.9$ Hz, 2H), 7.20 (d, $J = 7.9$ Hz, 2H), 2.70–2.53 (m, 2H), 1.60 (m, 2H), 1.43–1.18 (m, 18H), 0.89 (t, $J = 5.0$ Hz, 3H). ^{13}C NMR (75 MHz, CDCl$_3$) δ 146.57,

134.94, 128.04, 83.73, 36.33, 31.86, 31.46, 29.12, 25.00, 24.95, 22.74, 14.24.

2-Phenyl[1]benzothieno[3,2-b]benzothiophene (Ph-BTBT) and 2-(4-hexylphenyl)[1]benzothieno[3,2-b]benzothiophene (1b)

Compounds 5 (10 mmol), 7a or 7b (15 mmol), 2 M potassium carbonate and aliquat$_{336}$ were added to a 300 mL Schlenk flask. The mixture solution was degassed by purging with nitrogen for 30 min. Then Pd(PPh$_3$)$_4$ was added in one portion and the reaction mixture was heated at 105 $^\circ$C, and maintained at this temperature for 48 h while stirring. After cooling down to room temperature, the reaction mixture was poured into methanol. The gray precipitate was filtered off, washed with dilute hydrochloric acid, water and methanol. The crude product was further purified by sublimation to obtain white crystals Ph-BTBT and C6-Ph-BTBT. Ph-BTBT:[17] ^{1}H NMR (400 MHz, CDCl$_3$) δ 8.13 (d, $J = 1.1$ Hz, 1H), 7.99–7.87 (m, 3H), 7.75–7.66 (m, 3H), 7.53–7.35 (m, 5H). ^{13}C NMR (101 MHz, CDCl$_3$) δ 143.23, 142.50, 140.89, 138.57, 133.89, 133.38, 133.30, 132.34, 129.09, 127.64, 127.50, 125.19, 125.09, 124.68, 124.21, 122.52, 121.93, 121.75. HRMS (+ESI) m/z calcd for C$_{20}$H$_{13}$S$_2$ (M + H)$^+$ 317.0459, found 317.0455. 1b: ^{1}H NMR (400 MHz, CDCl$_3$) δ 8.12 (d, $J = 1.3$ Hz, 1H), 7.95–7.87 (m, 3H), 7.69 (dd, $J = 8.3, 1.6$ Hz, 1H), 7.61 (d, $J = 8.1$ Hz, 2H), 7.47 (td, $J = 7.6, 1.1$ Hz, 1H), 7.44–7.38 (m, 1H), 7.30 (d, $J = 8.1$ Hz, 2H), 2.67 (t, $J = 7.8$ Hz, 2H), 1.72–1.61 (m, 2H), 1.45–1.25 (m, 6H), 0.91 (dd, $J = 8.8, 5.1$ Hz, 3H). HRMS (+ESI) m/z calcd for C$_{26}$H$_{25}$S$_2$ (M + H)$^+$ 401.1398, found 401.1386.

Fabrication and characterization of OTFT devices

OTFT devices were fabricated in the top-contact/bottom-gate configuration on highly doped n-type Si wafers with 250 nm thick SiO$_2$ thermally grown by dry thermal oxidation which served as substrates and the gate electrode. The wafers were washed with deionized water, acetone and isopropanol, and blown dry with N$_2$ gas. The wafers were irradiated with UV for 10 min. Then the surfaces of the wafers were treated with a self-assembling monolayer of OTS (8) by immersing the cleaned wafer substrate in 0.1 M solution of OTS (8) in toluene at 65 $^\circ$C for 30 min. The wafers were blown dry with N$_2$ gas after cleaning with toluene. A thin film (40 nm thick) of Ph-BTBT or C6-Ph-BTBT as the active layer was vacuum-deposited on the Si/SiO$_2$ substrates kept at 25, 60, 80, 100 or 120 $^\circ$C a rate of 1.0–2.0 Å s^{-1} under high vacuum ($\sim 2.0 \times 10^{-4}$ Pa). On top of the organic thin film, gold films (50 nm) as drain and source electrodes were deposited through a shadow mask. For a typical device, the drain–source channel width (W)/length (L) are 380 µm/38 µm, 580 µm/58 µm, 780 µm/78 µm, and 980 µm/98 µm. The OTFTs devices were annealed at 80, 100 and 120 $^\circ$C or without annealing. The characteristics of the OTFT devices were obtained at room temperature in dark ambient conditions using a Keithley 4200 semiconductor parameter analyzer. By employing the following formula, the field-effect mobility (μ_{FET}) was extracted from the saturation regime ($V_d = -40$ V) of the I_d:

$$I_d = (W/2L)\mu_{TFT}C_i(V_g - V_{th})^2$$

where, C_i indicates the capacitance of the SiO_2 insulator, and V_g and V_{th} represent the gate and threshold voltages, respectively. The current on/off (I_{on}/I_{off}) ratio was determined from the current I_d at $V_g = -60$ V and $V_g = 0$ V. The performances of the OTFTs are shown in Tables 1 and 2.

Acknowledgements

Notes and references

1 (a) *Organic Electronics, Manufacturing and Applications*, ed. H. Klauk, Wiley-VCH, Weinheim, 2006; (b) *Organic Field-Effect Transistors*, ed. Z. Bao and J. Locklin, CRC Press, Boca Raton, 2007; (c) *Organic Electronics II: More Materials and Applications*, ed. H. Klauk, Wiley-VCH, Weinheim, 2012.

2 J. M. Adhikari, K. Vakhshouri, B. D. Calitree, A. Hexemer, M. A. Hickner and E. D. Gomez, *J. Mater. Chem. C*, 2015, **3**(34), 8799–8803.

3 (a) K. Takimiya, H. Ebata, K. Sakamoto, T. Izawa, T. Otsubo, T. Otsubo and Y. Kunugi, *J. Am. Chem. Soc.*, 2006, **128**(39), 12604–12605; (b) H. Ebata, T. Izawa, E. Miyazaki, K. Takimiya, M. Ikeda, H. Kuwabara and T. Yui, *J. Am. Chem. Soc.*, 2007, **129**(21), 15732–15733.

4 (a) A. Y. Amin, A. Khassanov, K. Reuter, T. Meyer-Friedrichsen and M. Halik, *J. Am. Chem. Soc.*, 2012, **134**(40), 16548–16550; (b) Y. Yuan, G. Giri, A. L. Ayzner, A. P. Zoombelt, S. C. Mannsfeld, J. Chen, D. Nordlund, M. F. Toney, J. Huang and Z. Bao, *Nat. Commun.*, 2014, **5**, 3005.

5 (a) H. Iino and J. Hanna, *Adv. Mater.*, 2011, **23**(15), 1748–1751; (b) N. Onojima, I. Shintani, S.-i. Kitahara, T. Takahashi, T. Kato and Y. Haramoto, *Phys. Status Solidi C*, 2011, **8**(2), 607–609; (c) A. J. van Breemen, P. T. Herwig, C. H. Chlon, J. Sweelssen, H. F. Schoo, S. Setayesh, W. M. Hardeman, C. A. Martin, D. M. de Leeuw, J. J. Valeton, C. W. Bastiaansen, D. J. Broer, A. R. Popa-Merticaru and S. C. Meskers, *J. Am. Chem. Soc.*, 2006, **128**(7), 2336–2345; (d) E. Lim, Y. M. Kim, J.-I. Lee, B.-J. Jung, N. S. Cho, J. Lee, L.-M. Do and H.-K. Shim, *J. Polym. Sci., Part A: Polym. Chem.*, 2006, **44**(16), 4709–4721; (e) X. Liu, T. Usui and J. Hanna, *Chem. Mater.*, 2014, **26**(19),

5437–5440; (f) H. Iino and J.-i. Hanna, *J. Appl. Phys.*, 2011, **109**(7), 074505; (g) H. Iino, T. Usui and J. Hanna, *Nat. Commun.*, 2015, **6**, 6828; (h) A. Kim, K. S. Jang, J. Kim, J. C. Won, M. H. Yi, H. Kim, D. K. Yoon, T. J. Shin, M. H. Lee, J. W. Ka and Y. H. Kim, *Adv. Mater.*, 2013, **25**(43), 6219–6225; (i) G. K. Dutta, S. Guha and S. Patil, *Org. Electron.*, 2010, **11**(1), 1–9; (j) J.-i. Hanna, A. Ohno and H. Iino, *Thin Solid Films*, 2014, **554**, 58–63.

6 H. Iino, T. Usui, T. Kobori and J. I. Hanna, *Dig. Tech. Pap.–Soc. Inf. Disp. Int. Symp.*, 2012, **2012**, 497–500.

7 H. Meng, F. Sun, M. B. Goldfinger, G. D. Jaycox, Z. Li, W. J. Marshall and G. S. Blackman, *J. Am. Chem. Soc.*, 2005, **127**(8), 2406–2407.

8 H. Iino, T. Kobori and J. I. Hanna, *J. Non-Cryst. Solids*, 2012, **358**(17), 2516–2519.

9 (a) F. Garnier, A. Yassar, R. Hajlaoui, G. Horowitz, F. Deloffre, B. Servet, S. Ries and P. Alnot, *J. Am. Chem. Soc.*, 1993, **115**(19), 8716–8721; (b) K. Takimiya, I. Osaka, T. Mori and M. Nakano, *Acc. Chem. Res.*, 2014, **47**(5), 1493–1502.

10 (a) M. Saito, I. Osaka, E. Miyazaki, K. Takimiya, H. Kuwabara and M. Ikeda, *Tetrahedron Lett.*, 2011, **52**(2), 285–288; (b) B. Košata, V. Kozmík and J. Svoboda, *Collect. Czech. Chem. Commun.*, 2002, **67**(5), 645–664; (c) C. Niebel, Y. Kim, C. Ruzié, J. Karpinska, B. Chattopadhyay, G. Schweicher, A. Richard, V. Lemaur, Y. Olivier, J. Cornil, A. R. Kennedy, Y. Diao, W.-Y. Lee, S. Mannsfeld, Z. Bao and Y. H. Geerts, *J. Mater. Chem. C*, 2015, **3**(3), 674–685; (d) S. Ito, M. Wehmeier, J. D. Brand, C. Kübel, R. Epsch, J. P. Rabe and K. Müllen, *Chem.–Eur. J.*, 2000, **6**(23), 4327–4342; (e) Y. S. Yang, T. Yasuda, H. Kakizoe, H. Mieno, H. Kino, Y. Tateyama and C. Adachi, *Chem. Commun.*, 2013, **49**(58), 6483–6485.

11 (a) F. Nüesch and M. Grätzel, *Chem. Phys.*, 1995, **193**, 1–17; (b) H. Meng, J. Zheng, A. J. Lovinger, B. C. Wang, P. G. Van Patten and Z. Bao, *Chem. Mater.*, 2003, **15**, 1778–1787; (c) M.-C. Um, J. Kwak, J.-P. Hong, J. Kang, D. Y. Yoon, S. H. Lee, C. Lee and J.-I. Hong, *J. Mater. Chem.*, 2008, **18**, 4698–4703.

12 M. Cardona, W. Li, A. E. Kaifer, D. Stockdale and G. C. Bazan, *Adv. Mater.*, 2011, **23**(20), 2367–2371.

13 I. Dierking, *Textures of Liquid Crystals*, WILEY-VCH, Weinheim, 2003.

14 R. J. Bushby, S. M. Kelly and M. O'Neill, *Liquid Crystalline Semiconductors*, Springer Series in Materials Science, Springer-Verlag, Berlin, 2013, vol. 169.

15 R. L. Headrick, S. Wo, F. Sansoz and J. E. Anthony, *Appl. Phys. Lett.*, 2008, **92**(6), 063302.

16 (a) A. D. Becke, *J. Chem. Phys.*, 1993, **98**(7), 5648–5652; (b) G. A. Petersson, A. Bennett, T. G. Tensfeldt, M. A. Al-Laham, W. A. Shirley and J. Mantzaris, *J. Chem. Phys.*, 1988, **89**(4), 2193–2218; (c) G. A. Petersson and M. A. Al-Laham, *J. Chem. Phys.*, 1991, **94**(9), 6081–6090.

17 S. Inoue, H. Minemawari, J. Y. Tsutsumi, M. Chikamatsu, T. Yamada, S. Horiuchi, M. Tanaka, R. Kumai, M. Yoneya and T. asegawa, *Chem. Mater.*, 2015, **27**(11), 3809–3812.